

Evaluation of hollow fiber-based direct contact and vacuum membrane distillation systems using aspen process simulation

Guan, Guoqiang; Yang, Xing; Wang, Rong; Field, Robert; Fane, Anthony Gordon

2014

Guan, G., Yang, X., Wang, R., Field, R., & Fane, A. G. (2014). Evaluation of hollow fiber-based direct contact and vacuum membrane distillation systems using aspen process simulation. *Journal of Membrane Science*, 464, 127-139.

<https://hdl.handle.net/10356/79612>

<https://doi.org/10.1016/j.memsci.2014.03.054>

© 2014 Elsevier Ltd. This is the author created version of a work that has been peer reviewed and accepted for publication by *Journal of Membrane Science*, Elsevier Ltd. It incorporates referee's comments but changes resulting from the publishing process, such as copyediting, structural formatting, may not be reflected in this document. The published version is available at: [<http://dx.doi.org/10.1016/j.memsci.2014.03.054>].

Downloaded on 20 Jul 2024 11:34:26 SGT

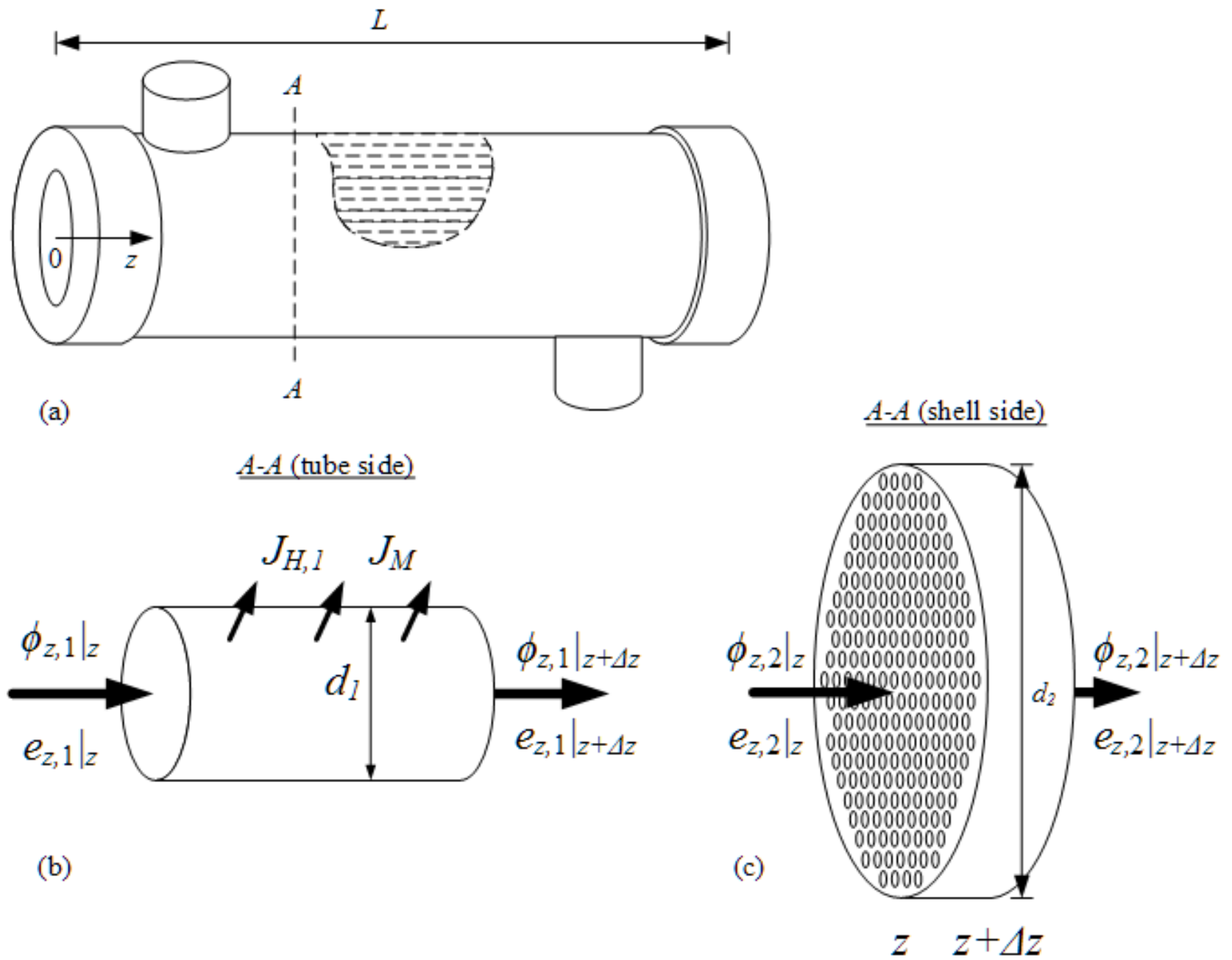


Fig.1 MD module schematic for DCMD and VMD configurations

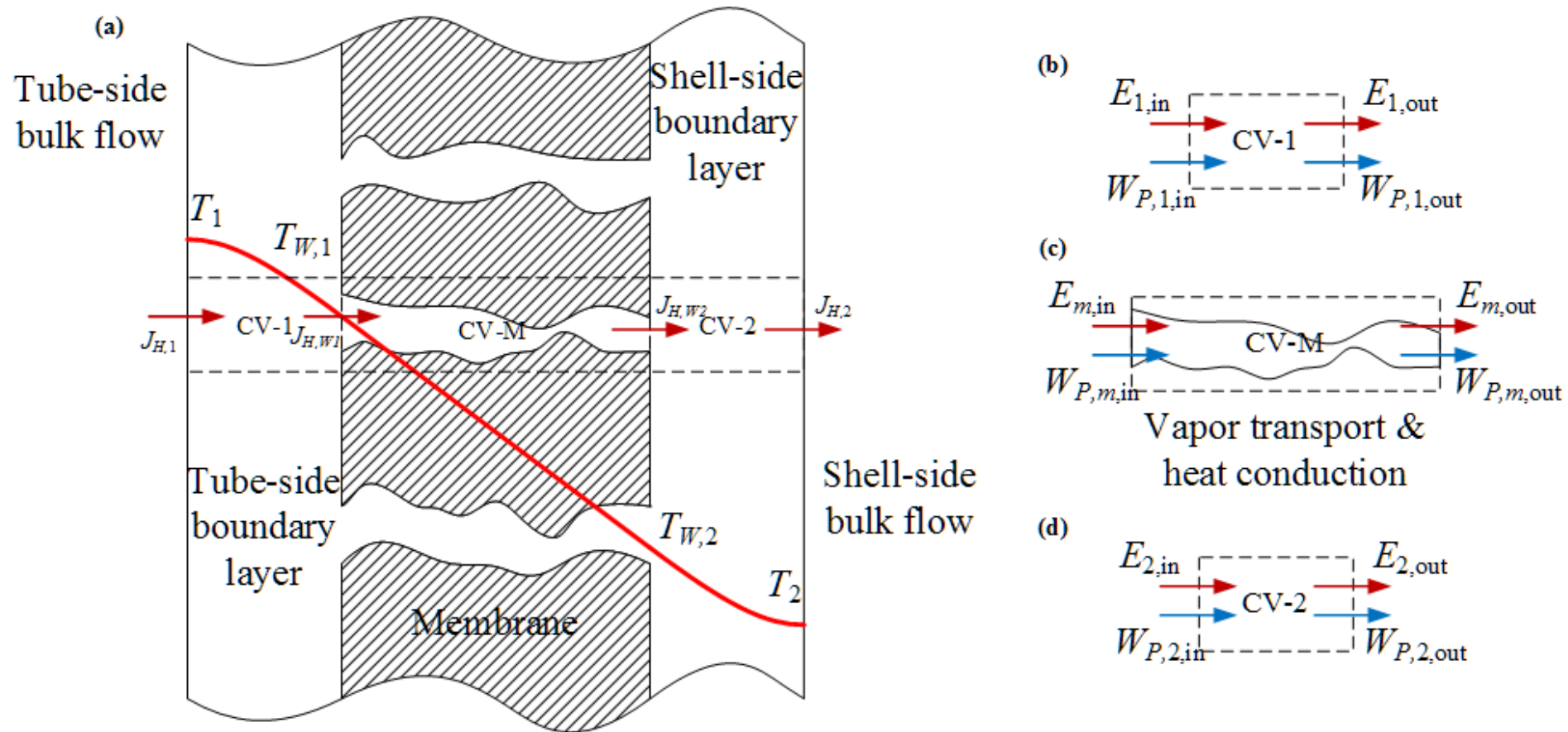


Fig.2 Schematic diagram of local heat and mass transfer MD heat and mass transfer adjacent to the membrane surface and across the membrane

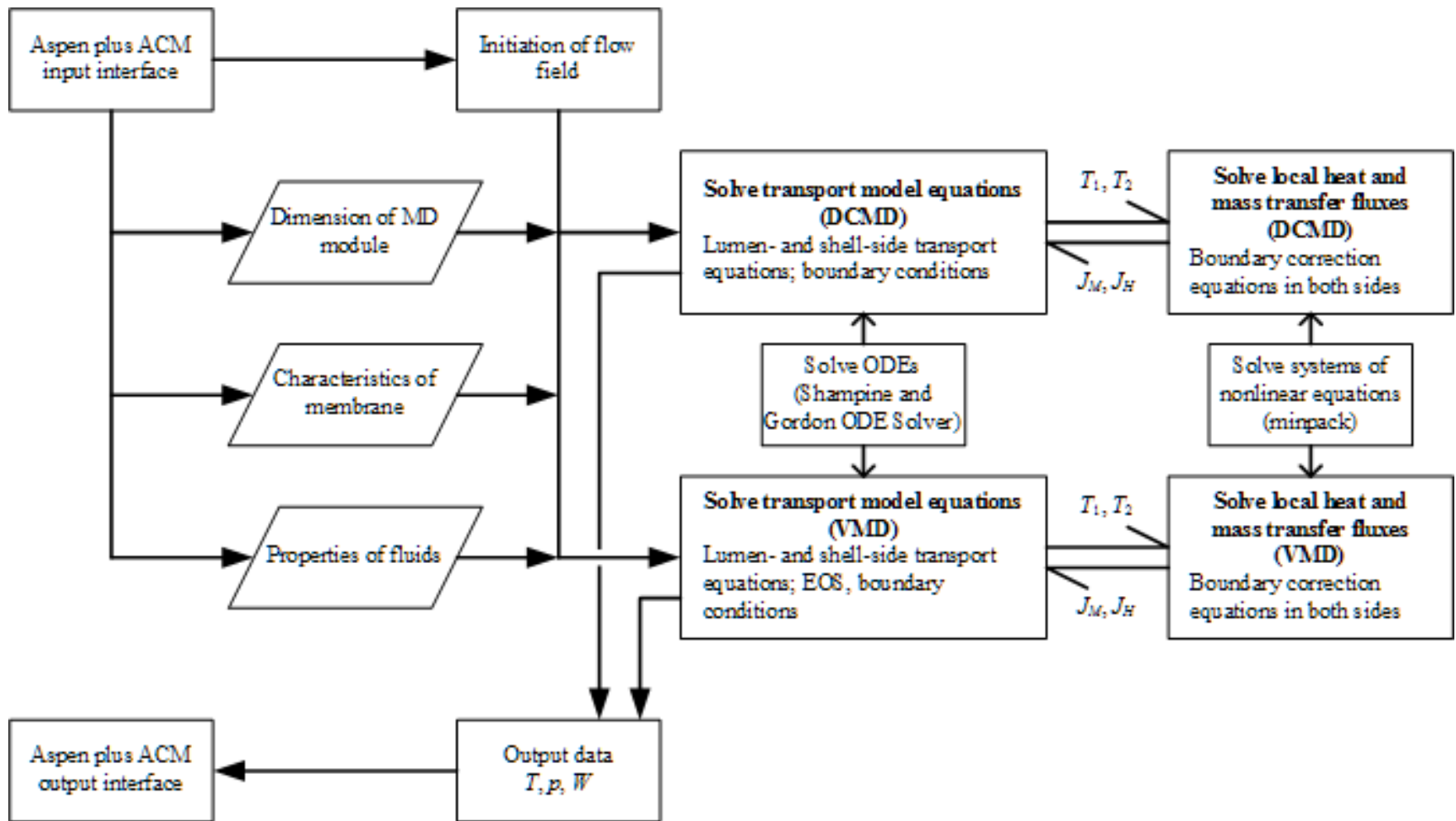


Fig.3 Computational flow chart for Aspen simulations of DCMD and VMD system

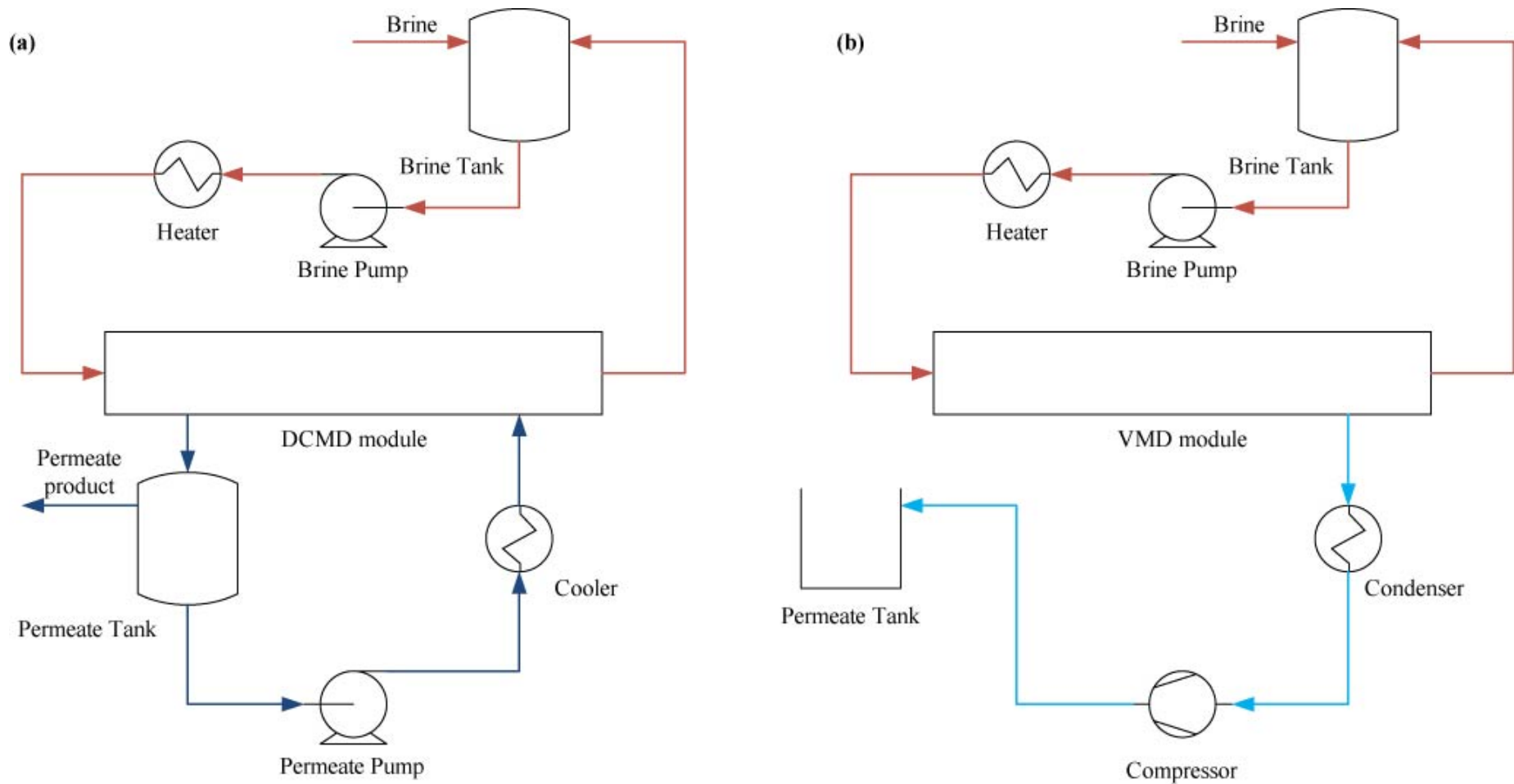


Fig.4 Flow sheets of MD systems in Aspen simulations (a) DCMD; (b) VMD

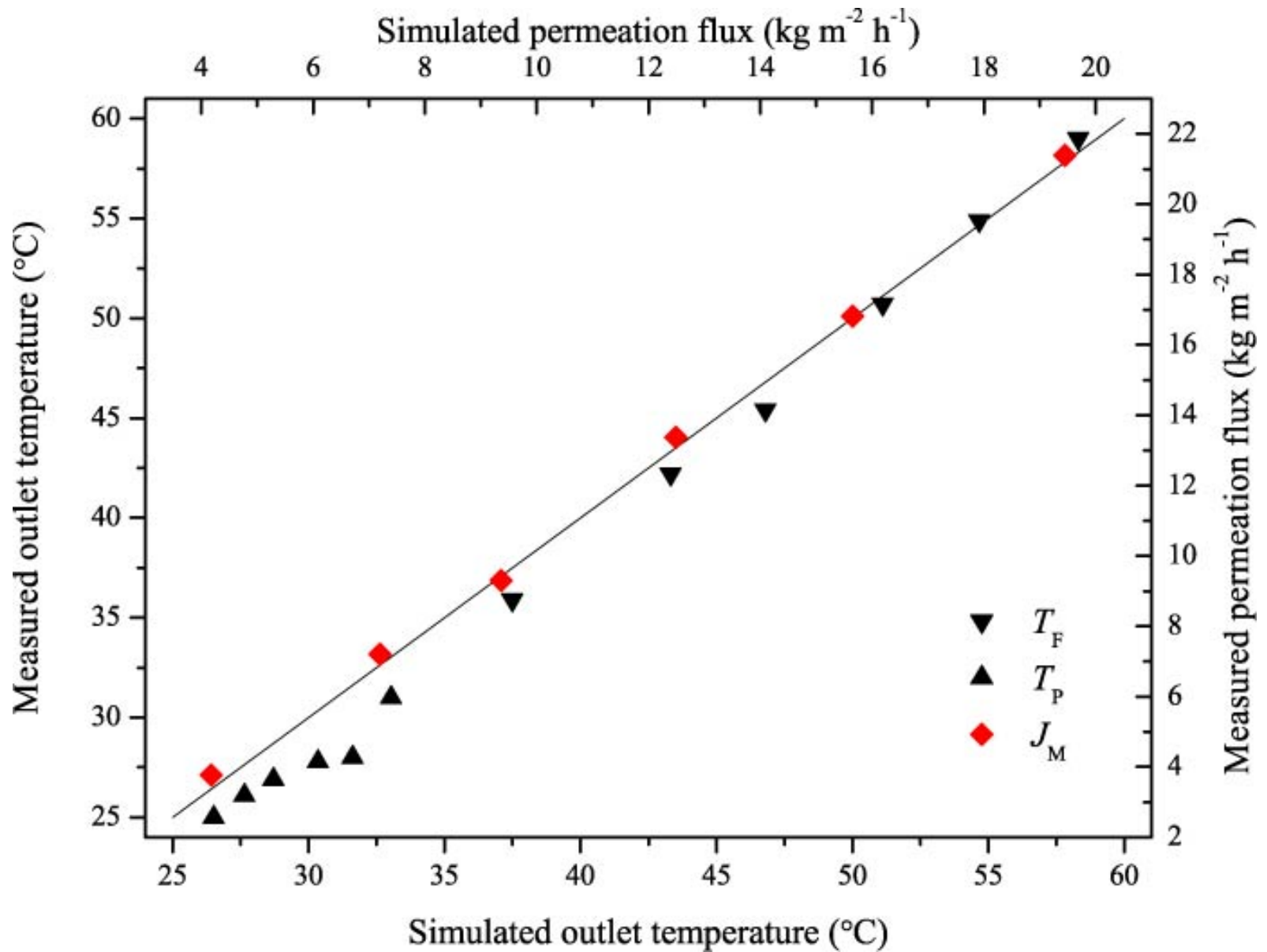


Fig.5 Comparison of permeation flux and outlet temperatures from simulation results and experimental data for DCMD module ($A_m = 180.9 \text{ cm}^2$, $T_{1,0} = 39.3\text{-}64.1 \text{ }^\circ \text{C}$ and $T_{2,0} = 23.5 \pm 0.5 \text{ }^\circ \text{C}$; $W_1 = 0.4 \text{ L}\cdot\text{min}^{-1}$ and $W_2 = 3 \text{ L}\cdot\text{min}^{-1}$)

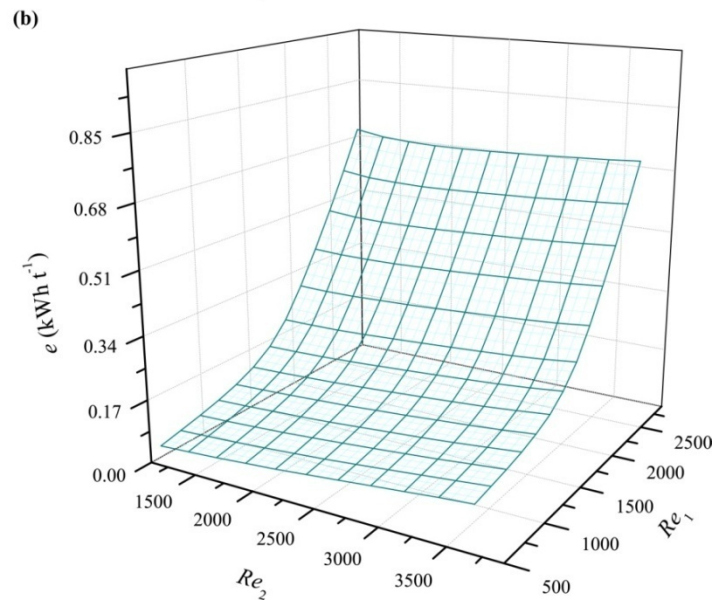
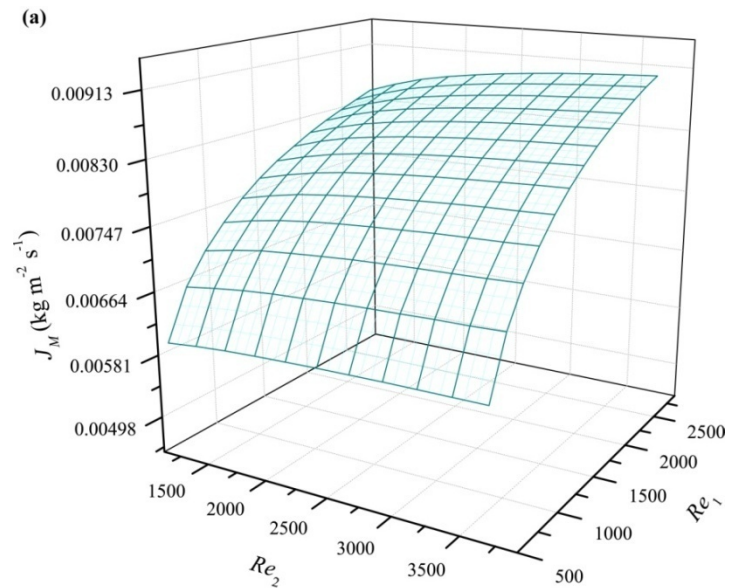


Fig.6 Effects of lumen- and shell-side flow conditions (Re_1 & Re_2) in simulated DCMD module on (a) Permeation flux; (b) Specific energy consumption (steady-state operation, feed: NaCl solution with initial feed concentration of 7.0 wt%, $T_{1,0} = 80^\circ \text{C}$ and $T_{2,0} = 30^\circ \text{C}$)

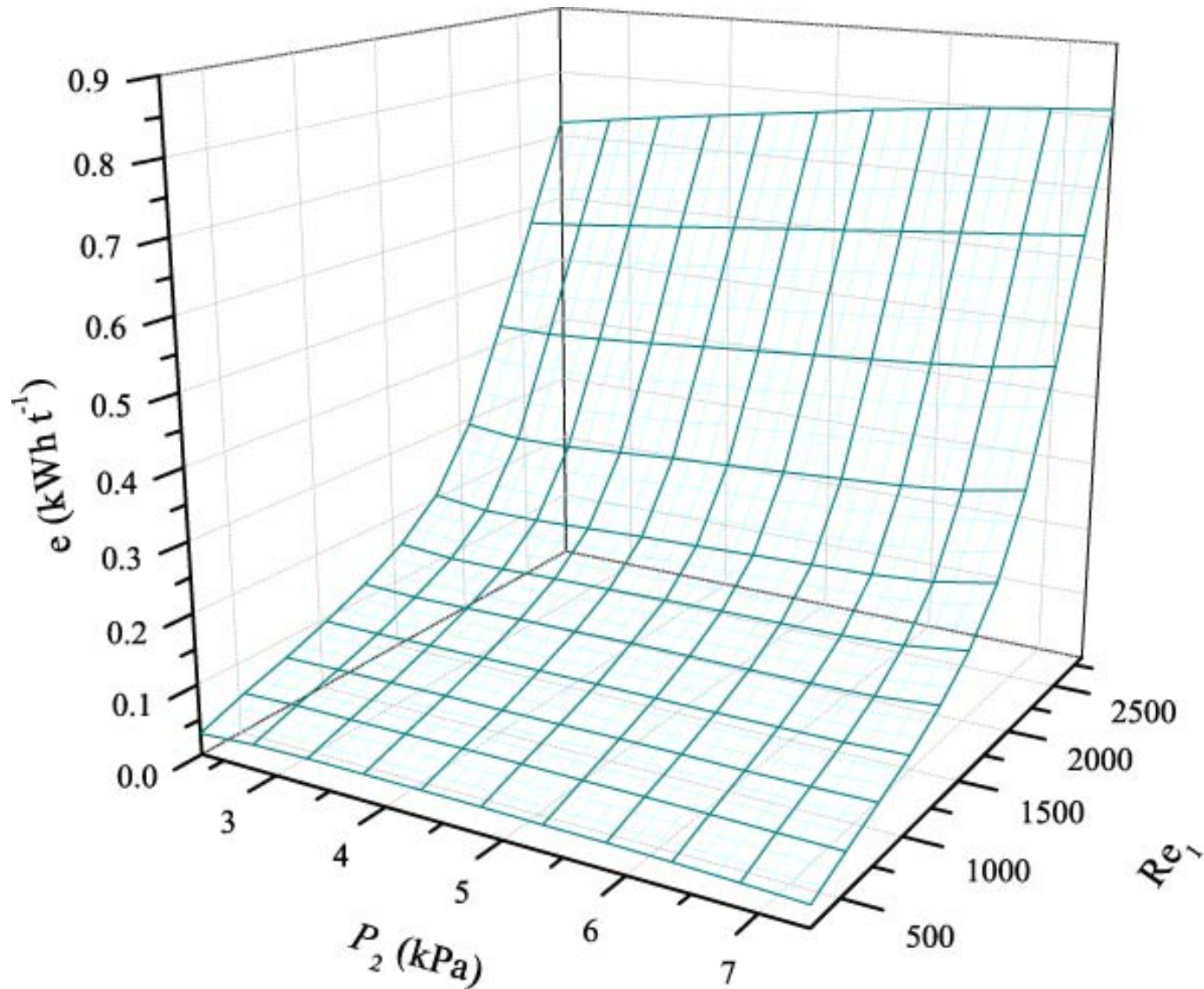


Fig.7 Specific energy consumption of simulated VMD system with varying vacuum pressure $p_{2,0}$ and lumen-side flow condition (Re_1) (steady-state operation, feed: NaCl solution with initial feed concentration of 7.0 wt%, $T_{1,0} = 80\text{ }^\circ\text{C}$, $p_{2,0}=2.3\sim 7.5\text{ kPa}$)

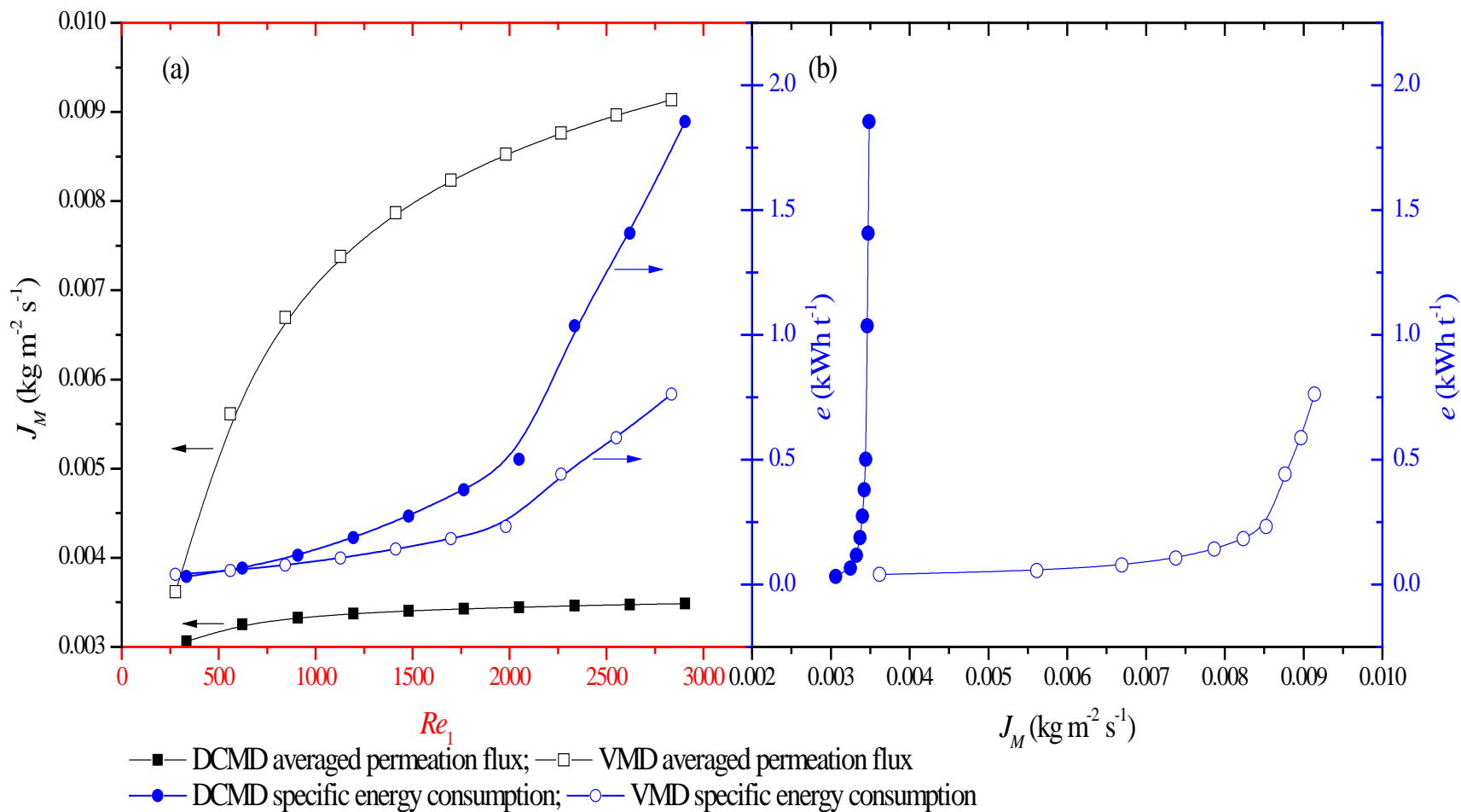


Fig.8 Specific energy consumption and permeation flux with varying Re_1 in simulated DCMD and VMD flowsheets (a) J_M and e vs. Re_1 , (b) e vs. J_M (steady-state operation, feed: NaCl solution with initial concentration of 7.0 wt%, $Re_2 = 456$, $T_{1,0} = 80^\circ\text{C}$ and $T_{2,0} = 30^\circ\text{C}$ for DCMD; $p_{2,0} = 4.25$ kPa for VMD)

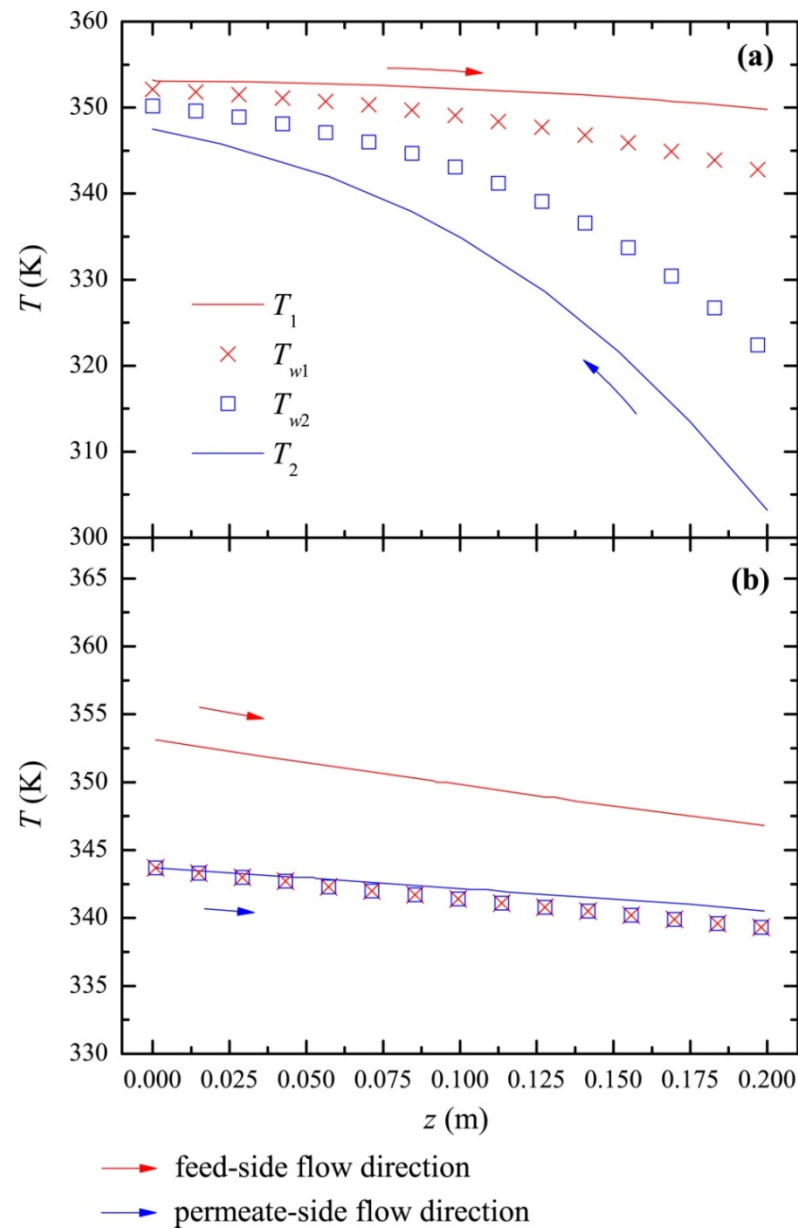


Fig.9 Simulated temperature profiles along the fiber length in the DCMD (a) and VMD (b) modules (steady-state operation, feed: NaCl solution with initial concentration of 7.0 wt%, $Re_1 = 1482$, $Re_2 = 456$, $T_{1,0} = 80^\circ\text{C}$ and $T_{2,0} = 30^\circ\text{C}$ for DCMD; $p_{2,0} = 4.25$ kPa for VMD)

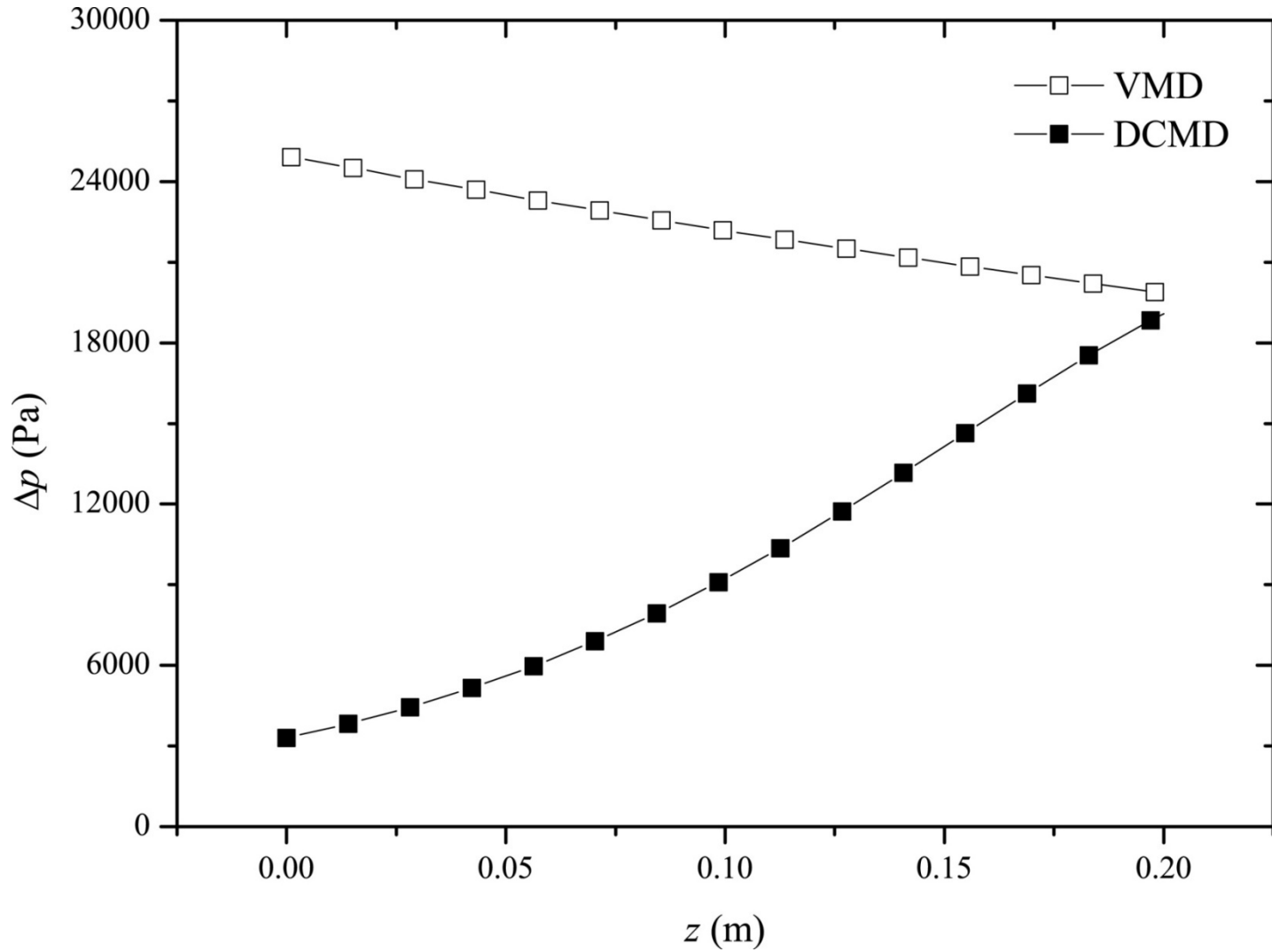


Fig.10 Simulated profiles of local driving force Δp along the fiber length in DCMD and VMD modules (steady-state operation, feed: NaCl solution with initial feed concentration of 7.0 wt%, $Re_1 = 1482$, $Re_2 = 456$, $T_{1,0} = 80$ °C and $T_{2,0} = 30$ °C for DCMD; $p_{2,0} = 4.25$ kPa for VMD)